



저작자표시-비영리-변경금지 2.0 대한민국

이용자는 아래의 조건을 따르는 경우에 한하여 자유롭게

- 이 저작물을 복제, 배포, 전송, 전시, 공연 및 방송할 수 있습니다.

다음과 같은 조건을 따라야 합니다:



저작자표시. 귀하는 원저작자를 표시하여야 합니다.



비영리. 귀하는 이 저작물을 영리 목적으로 이용할 수 없습니다.



변경금지. 귀하는 이 저작물을 개작, 변형 또는 가공할 수 없습니다.

- 귀하는, 이 저작물의 재이용이나 배포의 경우, 이 저작물에 적용된 이용허락조건을 명확하게 나타내어야 합니다.
- 저작권자로부터 별도의 허가를 받으면 이러한 조건들은 적용되지 않습니다.

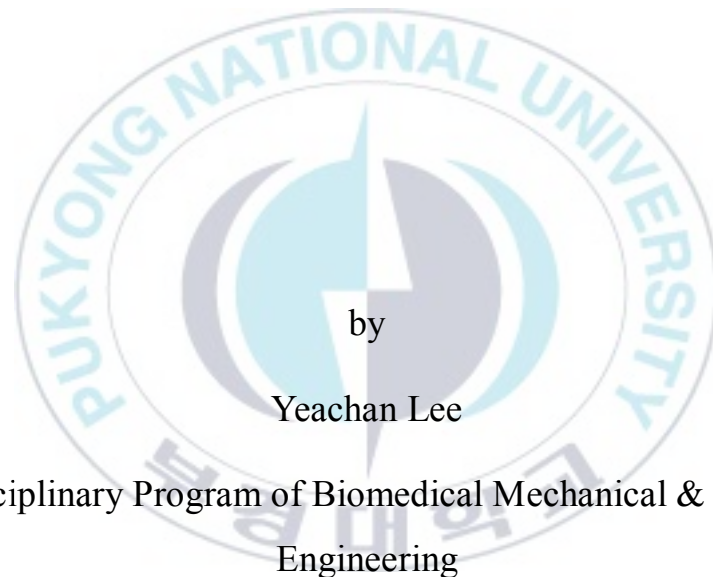
저작권법에 따른 이용자의 권리는 위의 내용에 의하여 영향을 받지 않습니다.

이것은 [이용허락규약\(Legal Code\)](#)을 이해하기 쉽게 요약한 것입니다.

[Disclaimer](#)

Thesis for the Degree of Master of Engineering

# **Low level laser therapy with marine derived material for fibrosis treatment**



by

Yeachan Lee

Interdisciplinary Program of Biomedical Mechanical & Electrical  
Engineering

The Graduate School

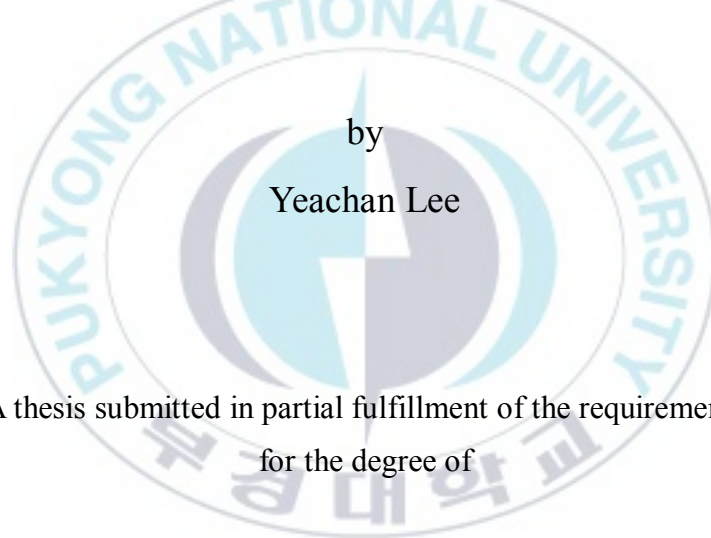
Pukyong National University

February 2020

# **Low level laser therapy with marine derived material for fibrosis treatment**

섬유증 치료를 위한 해양 유래 물질  
융합 저출력 레이저 치료법 연구

Advisor: Prof. Hyun Wook Kang



by

Yeachan Lee

A thesis submitted in partial fulfillment of the requirements  
for the degree of

Master of Engineering in Department of Spatial Information Engineering,  
The Graduate School,  
Pukyong National University

February 2020

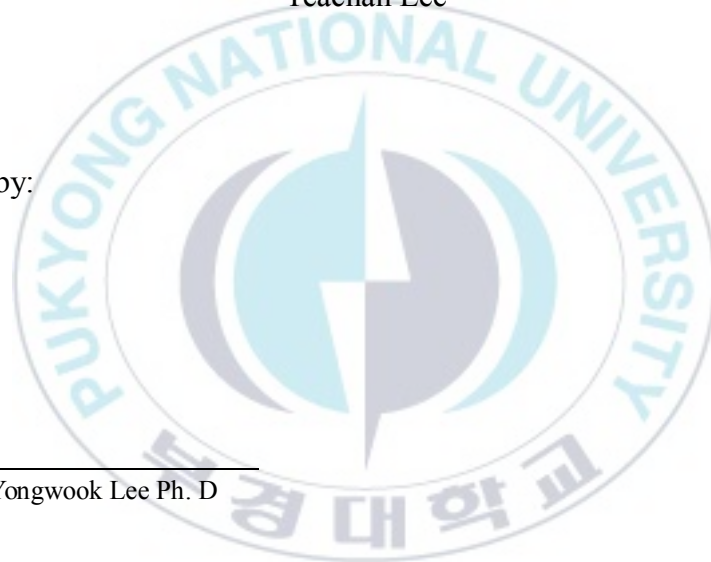
Low level laser therapy with marine derived material for fibrosis  
treatment

A dissertation

by

Yeachan Lee

Approved by:



\_\_\_\_\_  
(Chairman) Yongwook Lee Ph. D

\_\_\_\_\_  
(Member) Hyoung Shin Lee M. D

\_\_\_\_\_  
(Member) Hyun Wook Kang Ph. D

February 21, 2020

## **Low level laser therapy with marine derived material for fibrosis treatment**

**Yeachan Lee**

**Interdisciplinary Program of Biomedical Mechanical & Electrical Engineering**

**The Graduate School**

**Pukyong National University**

### **Abstract**

섬유증은 상처의 회복 과정이나 재형성 과정에서 세포 외 기질의 과도한 축적으로 형성된다. 섬유증은 신체의 거의 모든 부분에서 발생 할 수 있으며, 기관 및 조직의 기능을 저하하고 선진국 사망률의 절반에 병리학적 영향을 주는 흔한 질병이다. 현재까지 섬유증을 치료하기 위한 다양한 연구가 이루어졌지만, 아직 치료법이 부족하고 완치가 어려운 실정이다. 최근 저출력 레이저 치료 (low level laser therapy)가 다양한 의료 분야에서 적용되어 연구되고 있다. 저출력 레이저 치료란 가시광선 영역의 레이저를 낮은 출력으로 조사하여, 물리적인 손상 없이 생체 반응을 조절하는 방법이다. 저출력 레이저를 이용한 연구가 많이 이루어지고 있으나, 작용 기전이 명확하지 못할 뿐만 아니라 감소 및 억제 효과에 관한 연구 또한 부족한 실정이다. 따라서, 본 연구에서는 해양 유래 물질인 플로로글루시놀 (phloroglucinol)을 융합한 저출력 레이저의 섬유증 치료 효과와 그 가능성을 조사하였다. 생체 외 실험을 통해 플로로글루시놀 융합 저출력 레이저의 섬유화 인자 및 유도 인자의 발현 조절과 단독 치료보다 효과적인 감소 효과가 있음을 확인하였다. 또한, 동물 모델을 이용한 생체 내 실험을 통해 융합 치료 기술의 안전성과 유효성을 평가하고 섬유화 조직의 효과적인 감소 효과를 확인하였다. 결과적으로 해양 물질을 융합한 저출력 레이저 치료의 접근은 섬유증을 효과적으로

치료할 수 있고 현 치료법의 대안이 될 가능성이 있다. 나아가 섬유화 조절 효과의 더욱 명확한  
기전과 후속 재발 방지를 위한 연구가 이루어져야 할 것으로 여겨진다.



## Table of contents

<b>Abstract</b> .....	<b>i</b>
<b>Table of contents</b> .....	<b>iii</b>
<b>List of figures</b> .....	<b>vi</b>
<b>1. Introduction</b> .....	<b>1</b>
<b>1.1. Fibrosis</b> .....	<b>1</b>
<b>1.2. Overview of low level laser therapy</b> .....	<b>4</b>
<b>2. Phloroglucinol-assisted low level laser therapy for fibrosis treatment</b> ..	<b>7</b>
<b>2.1. Purpose</b> .....	<b>7</b>
<b>2.2. Materials and methods</b> .....	<b>8</b>
<b>2.2.1. Cell culture and combined treatment</b> .....	<b>8</b>
<b>2.2.2. MTT and BrdU assay</b> .....	<b>11</b>
<b>2.2.3. Wound healing assay for cell migration</b> .....	<b>11</b>
<b>2.2.4. Confocal immunofluorescence</b> .....	<b>12</b>
<b>2.2.5. Western blot analysis and collagen assay</b> .....	<b>13</b>

2.2.6. Statistical analysis	15
2.3. Results	16
2.3.1. Absorbance of phloroglucinol solution	16
2.3.2. Cell viability and proliferation	16
2.3.3. Comparison of wound closure rate	17
2.3.4. Gene expression of fibrotic markers	22
3. Effects of combined treatment of LLLT and phloroglucinol in a burn scar animal model	27
3.1. Purpose	27
3.2. Materials and methods	28
3.2.1. Fabrication of burn scar animal model	28
3.2.2. Laser and material treatment	29
3.2.3. Histological analysis	31
3.2.4. Statistical analysis	31
3.3. Results	32
3.3.1. Wound healing effect	32

3.3.2. Comparison of skin thickness and collagen distribution -----	35
4. Discussion -----	39
5. Summary -----	45
6. References -----	46



## List of figures

<b>Figure 1.</b> Overview of wound repair and fibrosis (Wynn, Thomas A., and et al. 2012) -----	3
<b>Figure 2.</b> Cell signaling pathways induced by LLLT (Hamblin, Michael R., and et al. 2006) -----	6
<b>Figure 3.</b> Absorbance spectra of phloroglucinol diluted in distilled water at various concentrations -----	10
<b>Figure 4.</b> Cell viability of (A) low level laser therapy (635nm for 30 seconds) at various power levels and (B) phloroglucinol at various concentrations -----	19
<b>Figure 5.</b> Effects of phloroglucinol assisted low level laser therapy (LLLT) on NIH/3T3 fibroblasts viability -----	20
<b>Figure 6.</b> (A) Microscopic images captured at 0 and 24 hours after cell wounding and (B) wound closure rate measured by using wound closure (%) = Migration cell surface area/total surface area 100% -----	21
<b>Figure 7.</b> Effects of phloroglucinol assisted low level laser therapy (LLLT) on transition -----	24

<b>Figure 8.</b> Effects of phloroglucinol assisted low level laser therapy (LLLT) on expressions of (A) $\alpha$ smooth muscle actin ( $\alpha$ SMA), (B) transforming growth factor (TGF) $\beta$ 1, and (C) type 1 collagen -----	2	5
<b>Figure 9.</b> The expressions of pro collagen 1 alpha 1 and the major component of type 1 collagen were measured by using optical density (OD) values from the standard curve -----	26	
<b>Figure 10.</b> Experimental conditions and design for combined treatment in a burn scar animal model -----	30	
<b>Figure 11.</b> Top-view images of wound in burn scar animal model -----	33	
<b>Figure 12.</b> Comparison of wound size after combined treatment -----	34	
<b>Figure 13.</b> Hematoxylin and eosin staining of normal skin and treated tissues for histological features after 3 weeks -----	36	
<b>Figure 14.</b> Quantitative analysis of skin layer thickness (dermis and epidermis) after 3 weeks -----	37	
<b>Figure 15.</b> Masson's trichrome staining of normal skin and treated tissue for collagen formation after 3 weeks -----	38	

# 1. Introduction

## 1.1. Fibrosis

Fibrosis is a highly prevalent disease, which has pathological effect to 45 % of deaths in developed countries. Fibrosis is a pathological feature of most chronic inflammatory diseases. Fibrosis affects almost every tissue and organ in the body and leads to organ malfunction and ultimately death. Fibrosis also influences tumor invasion and metastasis, and the pathogenesis of many progressive myopathies. Fibrosis is formed by excessive fibrous connective tissue in inflamed or damaged tissue. Fibrosis results from excessive extracellular matrix (ECM) deposition and collagen formation during wound healing (Figure 1) [1]. The main mechanism of fibrosis involves the transition of fibroblasts to myofibroblasts, which is caused by a transforming growth factor  $\beta$ 1 (TGF  $\beta$ 1). TGF  $\beta$ 1 is a key molecular factor of fibrosis [1, 2]. A general healing response to injury or stress relates TGF  $\beta$ 1. Recent studies demonstrated that the myofibroblasts, which induced by TGF  $\beta$ 1, play an essential role in fibrotic diseases. Induced myofibroblasts increase fibrotic markers, such as  $\alpha$  smooth muscle actin ( $\alpha$  SMA) and collagen [1, 3-5]. Currently, some conventional medical options are used for fibrosis treatment. However, current treatments merely can slow the progression of fibrosis and there aren't complete treatment because of complex pathogenesis and a

high recurrence rate [6]. Therefore, many researches of fibrosis have focused on elucidating the molecular and immunological mechanisms.



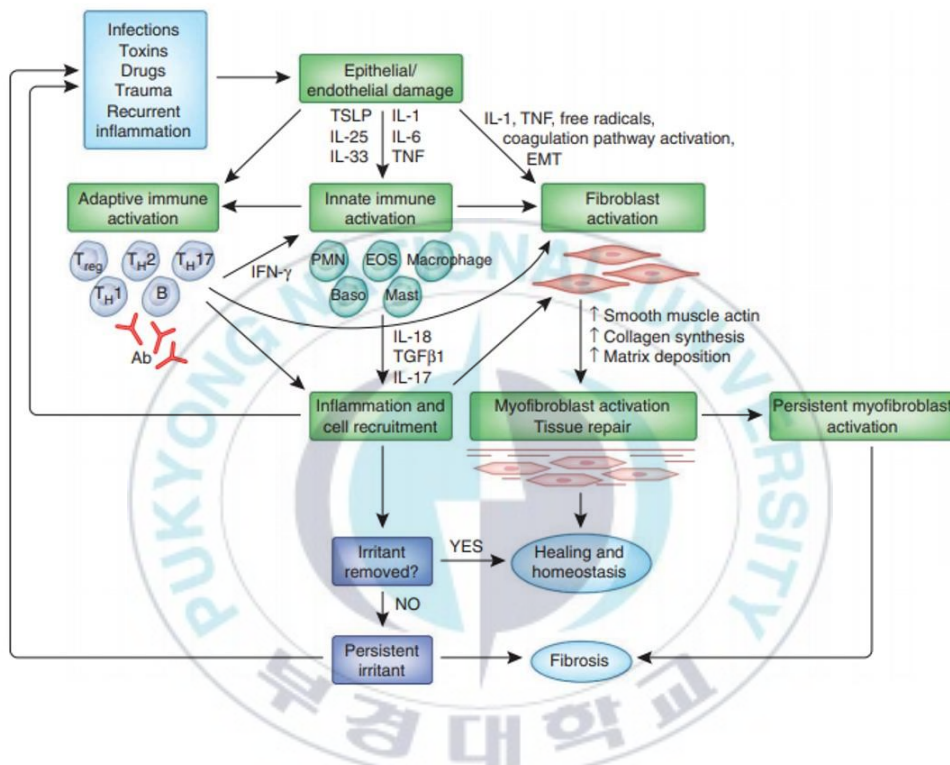


[Figure adopted from Ref. (Wynn, Thomas A., and Thirumalai R. Ramalingam. "Mechanisms of fibrosis: therapeutic translation for fibrotic disease." Nature medicine 18.7 (2012): 1028.)]

Figure 1. Overview of wound repair and fibrosis

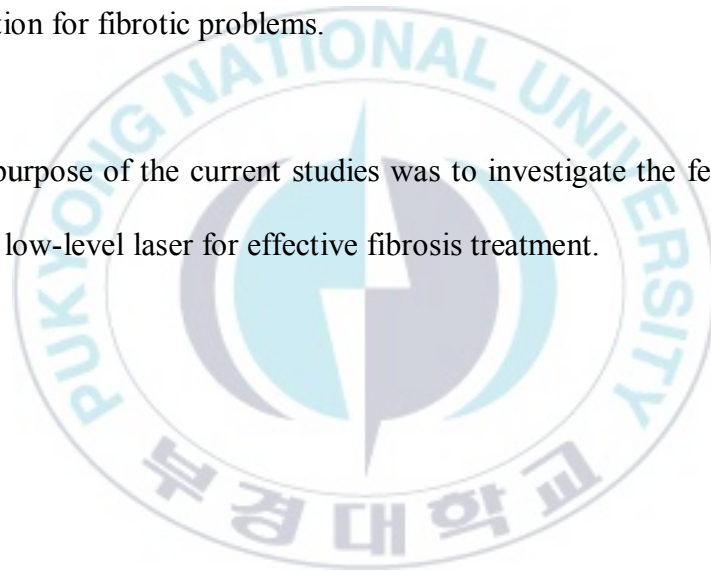
## 1.2. Overview of low level laser therapy

The first trial of low-level laser irradiation was discovered by Dr. Endre Mester in 1967 [7]. The attempt of low powered 694 nm laser light has shown an effect of hair growth in mice. For several decades, low-level laser with coherent laser light was used in medical parts. Nowadays non-coherent light also studied and used for treatment. Low-level laser therapy (LLLT), also called photobiomodulation, is a promising method for the treatment as a noninvasive and nonthermal methods [5, 8-10]. LLLT typically delivers a range of wavelengths from 600 to 1000 nm under 500 mW without thermal effect using laser diodes or LEDs [11, 12]. In common, red lights are often used to accelerate wound healing and to reduce inflammation [8, 13]. Photon absorption by cytochrome c (CCO) is the main mechanism of LLLT on cellular functions. CCO plays a critical role in oxygen metabolism and ATP production (Figure 2). LLLT can improve cell oxygen metabolism by increasing the concentration of CCO, which lead a longer lasting metabolic effect [14, 15]. Moreover, LLLT can regulate molecule-dependent biological processes such as cell proliferation, migration, and expression of growth factors and cytokines [7, 16].

A recent study reported that LLLT with 635 nm wavelength could reduce fibrotic activities in transition-induced fibroblast cells [9]. In addition, 635 nm

light has an anti-inflammatory effect by modulating prostaglandin E2 production and cyclo-oxygenase 1 and 2 mRNA expression [7]. Therefore, LLLT is a feasible therapeutic approach for fibrosis treatment in a noninvasive and nonthermal manner without any physical changes in tissue. However, the molecular and cellular underlying mechanism of LLLT is still under investigation, and there is room to improve the therapeutic efficacy of biostimulation for fibrotic problems.

Thus, the purpose of the current studies was to investigate the feasibility and efficacy of low-level laser for effective fibrosis treatment.



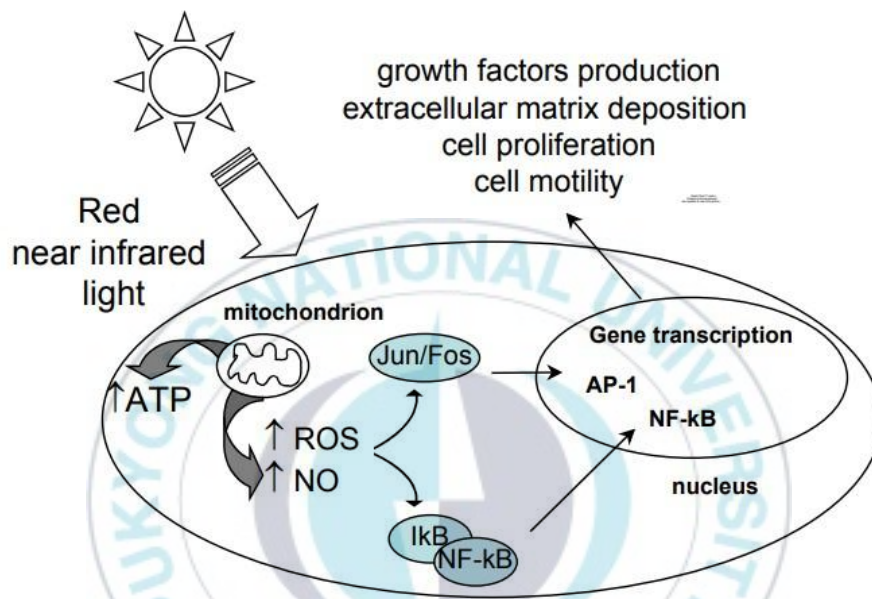


[Figure adopted from Ref. (Hamblin, Michael R., and Tatiana N. Demidova. "Mechanisms of low level light therapy." Mechanisms for low-light therapy. Vol. 6140. International Society for Optics and Photonics, 2006.)]

Figure 2. Cell signaling pathways induced by LLLT

## 2. Phloroglucinol-assisted low level laser therapy for fibrosis treatment

### 2.1. Purpose

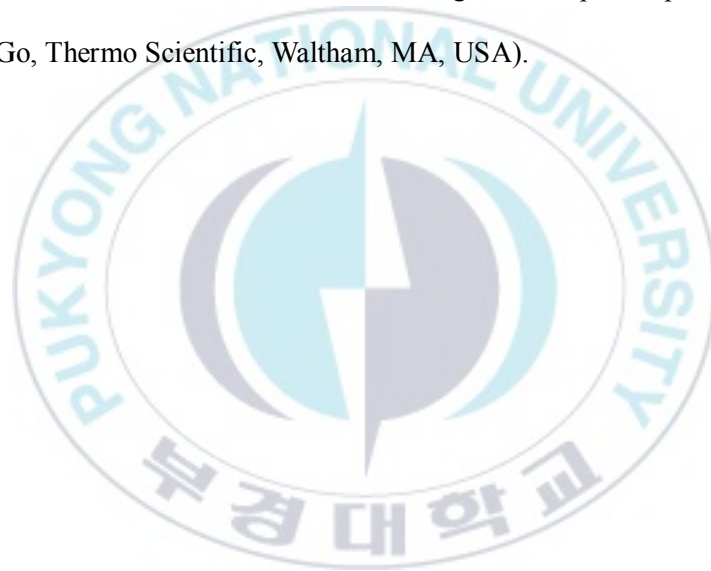
The purpose of the current study was to investigate and develop an effective combined treatment for fibrosis by targeting fibrotic markers using phloroglucinol (PHL) and LLLT. It was hypothesized that the combined effect could modulate the transition of fibroblasts and eventually minimize fibrotic expressions. Recent studies demonstrated that PHL has antifibrotic and antiinflammatory effects on fibroblast cells [17]. PHL has been widely studied and already used for pharmaceutical effect to treat gallstones and gastrointestinal disorders [18, 19]. In addition, PHL forms phlorotannin that inhibits fibrosis by modulating the expression of TGF,  $\alpha$ -SMA, and myofibroblast transition [20]. Thus, the application of biocompatible marine-derived PHL is a feasible material-based treatment for fibrotic diseases, such as tracheal stenosis. The current study examined various combinations of PHL and LLLT *in vitro* for comparison of cellular responses and evaluated cell viability and proliferation in a qualitative and quantitative manner. To identify the degree of the enhanced treatment, western blotting was used to assess the expression levels of  $\alpha$ -SMA, TGF- $\beta$ , and collagen type I in fibroblast cells after treatment.

## 2.2. Materials and Methods

### 2.2.1. Cell culture and combined treatment

NIH/3T3 murine embryonic fibroblasts (MEF) cells obtained from the Korean cell line bank were cultured in Dulbecco's modified Eagle's medium (DMEM, Corning, NY, USA) containing 10 % bovine calf serum (BCS, Welgene, Korea) and 1 % anti-anti (Gibco, ThermoFisher, MA, USA) in a humidified incubator at 37 °C and with a 5 % CO<sub>2</sub> atmosphere. MEF cells at passages 6-8 were cultured in DMEM with 2 % fetal bovine serum (FBS, Corning) and 5 ng/ml human (TGF)- $\beta$ 1 (PeproTech, Rocky Hill, NJ, USA) to induce the differentiation of fibroblasts. The laser and material treatments were provided simultaneously or respectively after TGF- $\beta$ 1 was treated. LLLT was conducted by using a visible laser system (SD-635-HS-1W, CNI laser, China) with a 635 nm wavelength in continuous-wave mode. A frontal light distributor (Medlight, Switzerland) with a beam diameter of 16 mm was used to irradiate the incident light in a uniform distribution. Before testing, the laser power was measured using a power detector (PD-300-3W, Ophir, Jerusalem, Israel) and power meter (Nova , Ophir, Jerusalem, Israel). The laser light was irradiated for 30 s at five different power conditions to identify the optimal irradiation power: 25 mW (0.375 J/cm<sup>2</sup>), 50 mW (0.75 J/cm<sup>2</sup>), 100 mW (1.5 J/cm<sup>2</sup>), 200 mW (3.0 J/cm<sup>2</sup>), and 300 mW (4.5 J/cm<sup>2</sup>). To prevent any overlapping of the irradiated light due to scattering, cells were seeded apart (every two wells), and a black plate was used as a background to minimize specular

reflection. PHL (GPR grade, MB-P4706, MB Cell, Seoul, Korea) was dissolved in distilled water (10 mg/ml) and filtered twice by using a membrane filter. The PHL stock solution was injected in the medium at various concentrations (25, 50, 100, 200, 300, and 10,000  $\mu\text{g/ml}$ ) to identify the optimal concentration for cell treatment. For each concentration, the stock solution was diluted in distilled water to estimate the absorbance of PHL as a function of wavelength (Figure 3). The absorbance spectra were measured between 300 and 800 nm using a microplate spectrophotometer (Multiskan Go, Thermo Scientific, Waltham, MA, USA).



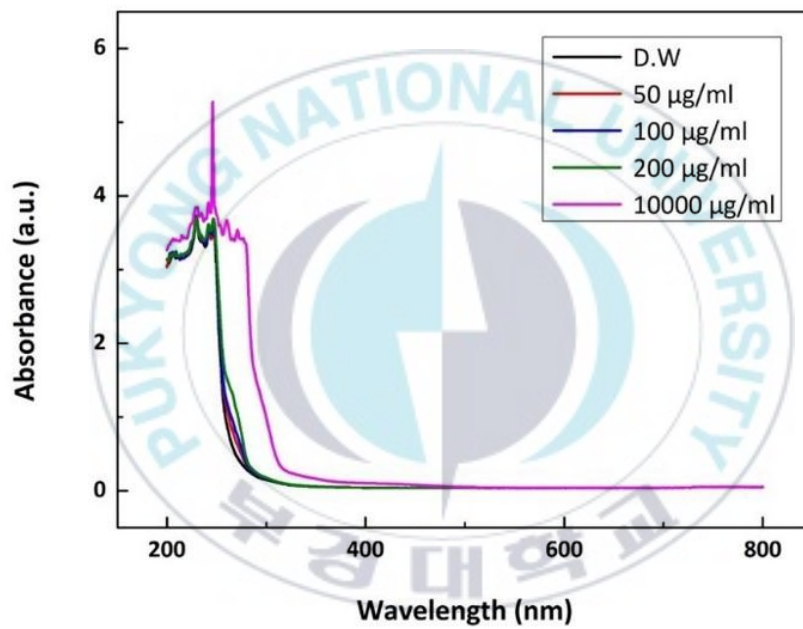


Figure 3. Absorbance spectra of phloroglucinol diluted in distilled water at various concentrations (50, 100, 200, and 10,000 ug/ml)

### **2.2.2. MTT and BrdU assay**

Cell viability and proliferation were evaluated using an MTT and BrdU cell proliferation assay kit (#6813S, Cell Signaling Technology, Danvers, USA). MEF cells were seeded into 96-well plates ( $8 \times 10^3$  cells/well) in DMEM with 10 % BCS. After 24 h of incubation, DMEM was replaced with 2 % FBS medium with or without TGF- $\beta$ 1. Five different conditions were evaluated: control, TGF-treated, PHL only, laser only, and PHL-assisted laser. After preparation, the cells were tested and then incubated for 24 and 48 h. For measuring cell viability after incubation for 4 h with 1 mg/ml MTT tetrazolium bromide solution (Sigma Aldrich, St. Louis, MO, USA), the DMSO was replaced to dissolve the MTT formazan. The absorbance was measured using a microplate spectrophotometer at a 540 nm wavelength. Based on the cell viability results, LLLT with 25 mW and 100  $\mu$ g/ml of PHL was selected for the combined treatment and used for the remaining experiments. For measuring cell proliferation, a BrdU cell proliferation kit was used following the instructions from the manufacturer (Cell Signaling Technology, Danvers, Massachusetts, USA).

### **2.2.3. Wound healing assay for cell migration**

MEF cells were seeded into 24-well plates ( $4 \times 10^4$  cells/well) in DMEM with 10 % BCS. After confluence was reached, cells were scratched using a scratcher (SPLScar scratcher, 0.5 mm tip size). After washing the cells with PBS, the medium was replaced with 2 % FBS DMEM with or without TGF- $\beta$ 1 and treatments with PHL only, laser only, and PHL-assisted laser were performed immediately. The images of the scratched

cell monolayers were captured after 24 h incubation time. The migration was quantified by dividing a migrated cell surface area by the total scratched surface area, which gives the percent closure (%) by using the MRI wound Healing Tool ([http://dev.mri.cnrs.fr/projects/imagej-macros/wiki/Wound\\_Healing\\_Tool](http://dev.mri.cnrs.fr/projects/imagej-macros/wiki/Wound_Healing_Tool)) plugin of ImageJ software (1.51J8, NIH, Bethesda, MD, USA). Images were converted into 32-bit grayscale and adjusted by using the enhance-contrast (normalize) and find-edges functions. After the images were set threshold, a wand tracing tool was used to detect the migrated cell surface area [21].

#### **2.2.4. Confocal immunofluorescence**

MEF cells were seeded on glass coverslips in 6-well plates (200000 cells per well) in DMEM with 10 % BCS, and the medium was replaced by 2 % FBS DMEM with or without TGF- $\beta$ 1. Then, 24 and 72 h after various treatments, the cells were fixed with 4 % formaldehyde in PBS for 15 minutes after a PBS wash. The fixed cells were permeabilized with 0.1 % Triton X-100 in PBS for 10 minutes and blocked with 1 % BSA in PBS (Tecknova, Dartmouth, USA) for an hour. Primary antibodies diluted in 1 % BSA, mouse monoclonal anti-alpha smooth muscle actin ( $\alpha$ -SMA, 1:100, Abcam) and rabbit polyclonal anti-collagen 1 (1:500, Abcam) were incubated overnight at 4 °C. Secondary antibodies diluted in 1 % BSA, anti-mouse (Alexa 488 pre-adsorbed, Abcam), and anti-rabbit (Alexa 405, Abcam) were incubated for an hour at room temperature. The nuclei were stained with propidium iodide (PI, 1:100, Sigma). All

images were captured using a confocal laser scanning microscope (LSM 700, ZEISS, Germany). Sequential scanning was used for double labelling to avoid crosstalk between channels. Densitometric analysis of the intensity was performed using ImageJ software. To correct the uneven background, the rolling ball method of background subtraction was performed by using the split channels and subtract background functions. Each image converted into 8-bit grayscale and ROI (Regions of interest) were selected by using a selection tool. Mean gray values were measured to compare the fluorescence intensity. It should be noted that fluorescence excitation/emission may not be a linear process and the CCD sensor responsivity is merely linear from the NEE (Noise equivalent exposure) to the SEE (Saturation equivalent exposure). However, the current densitometric analysis still enabled the relative comparison under the same conditions [22].

#### **2.2.5. Western blot analysis and collagen assay**

Western blot analysis was used to confirm the protein expression levels of  $\alpha$ -SMA, TGF- $\beta$ , and collagen in fibroblast cells after all treatments. After two PBS washes, cells were collected and lysed in lysis buffer [50 mmol/L Tris-HCl (pH 7.5), 250 mmol/L NaCl, 0.5 % TritonX-100, 1 mmol/L EDTA, 1 % phosphatase inhibitor, 1 % protease inhibitor (Sigma, St, Louis, MO)] at 4 °C for 30 minutes. The protein was centrifuged at 12,000 rpm for 15 minutes at 4 °C and quantified using a BCA protein assay kit (ThermoFisher). Lysate containing 30  $\mu$ g of protein was separated by sodium dodecyl

sulfate-polyacrylamide (SDS-PAGE) and transferred to a PVDF membrane (Bio-Rad, Hercules, CA, USA) at 300 mA for 90 minutes. The membranes were blocked with 5 % BSA for 1 h and incubated with diluted, primary antibodies for  $\alpha$ -SMA (1:1000), TGF- $\beta$  (1:1000), collagen (1:1000), and  $\beta$ -actin (1:5000; Sigma Chemical Co, USA) at 4 °C overnight. After washing the cells three times with TBS-T buffer [20 mM Tris (pH 7.4), 150 mM, NaCl, 0.1 % Tween-20], the membranes were incubated with secondary antibodies diluted with HRP-anti-rabbit and HRP-anti-mouse (1:3000, Santa Cruz, CA, USA). An image analyzer (In-vivo FX; Kodak, Canada) with a detection solution (Amersham ECL Western blotting detection reagents; GE Healthcare, Pittsburgh, PA, USA) was used to evaluate the signals, and the protein expression was quantified with ImageJ gel analysis plugin (<https://lukemiller.org/index.php/2010/11/analyzing-gels-and-western-blots-with-image-j/>). Band images were converted into 8-bit grayscale and selected the first lane by using rectangular selection tool. After the next lane was selected, the plot lanes function was used to generate the lane profile plots. The peak of interest was measured from the closed area by using a straight line on the base of plots and a wand tool. To quantify the degree of collagen generation, we used a Mouse pro-collagen 1 alpha 1 ELISA kit and followed the manufacturer's instructions (Abcam, Cambridge, UK). A BCA protein assay was performed to quantify the protein in samples at 72 h, and all groups were tested three times.

### 2.2.6. Statistical analysis

Statistical analysis was performed by using SPSS software 22 (SPSS Inc, Chicago, IL, USA), which calculated mean  $\pm$  standard deviation for at least three independent experiments. The Mann-Whitney U test was used for nonparametric statistical analysis, and significance was considered at  $p < 0.05$ .



## 2.3. Results

### 2.3.1. Absorbance of phloroglucinol solution

The absorbance spectrum of PHL solution was evaluated in various conditions (0, 50, 100, 200, 10000 µg/ml). The peak absorbance of the PHL solution at various concentrations is near 250 nm, as shown in Figure 3. There was no absorbance after 500 nm—even at the 100 µg/ml concentration used for experimental conditions. In addition, the absorbance range of the PHL solution was between 200 and 300 nm. According to the PHL absorbance results, PHL will not absorb light from the laser treatment (635 nm wavelength). Thus, phloroglucinol-assisted LLLT is different from the photodynamic therapy that uses photochemical reaction by photosensitizer.

### 2.3.2. Cell viability and proliferation

MTT and BrdU assays were performed to confirm the toxicity and proliferation of the combined therapy. MEF cells were irradiated with LLLT or treated with PHL under various conditions and incubated for 24 h and 48 h. The control group had no treatment, and the TGF group was treated only with TGF-β1 for transition of fibroblasts. Cell viability for the TGF group was significantly increased compared to the control group (Figure 4). As shown in Figure 4A, LLLT showed no critical changes in cell viability and no toxicity at 24 h and 48 h. Although the LLLT groups yielded slight differences

in the cell viability, 25 mW was selected for the combined treatment due to its lowest cell viability and the minimum power to avoid any undesirable heat generation. In fact, the power level of 25 mW was used in the previous research of fibrosis inhibition using LLLT. For various concentrations of PHL, cell viability decreased and toxicity occurred over 200  $\mu\text{g/ml}$  at 24 h (Figure 4B). However, proliferation was decreased at the 100  $\mu\text{g/ml}$  concentration after 48 h without toxicity at 24 h. The optimized conditions (LLLT : 25 mW, irradiation time : 30 s, phloroglucinol concentration of 100  $\mu\text{g/ml}$ ) were used for the remaining experiments. Using the optimized conditions, cell viability (Figure 5A) and proliferation (Figure 5B) for all groups were not significantly changed at 24 h. The TGF group showed an increase in both, compared with the control. The cell viability and proliferation for The LLLT or PHL groups were reduced at 48 h. However, LLLT+PHL decreased the cell viability and the proliferation more than the PHL or LLLT groups did at 48 h, which was the same as the control. Therefore, PHL-assisted LLLT with 25 mW and at 100  $\mu\text{g/ml}$  was more effective in the inhibition of cell viability and proliferation than individual usage in this study.

### 2.3.3. Comparison of wound closure rate

A wound healing assay was performed (Figure 6) to analyze the effects of combined therapy on MEF cell migration. A wound scratch area was observed at 24 h after all treatments and compared to the control. Wound closure for the TGF group ( $76.8 \pm 3.8 \%$ ) was significantly improved compared to the control ( $55.9 \pm 4.2 \%$ ). However, wound

closure in the LLLT+PHL group ( $49.8 \pm 1.5 \%$ ) was reduced compared to the control.

Thus, PHL-assisted LLLT inhibited TGF-induced cell migration.



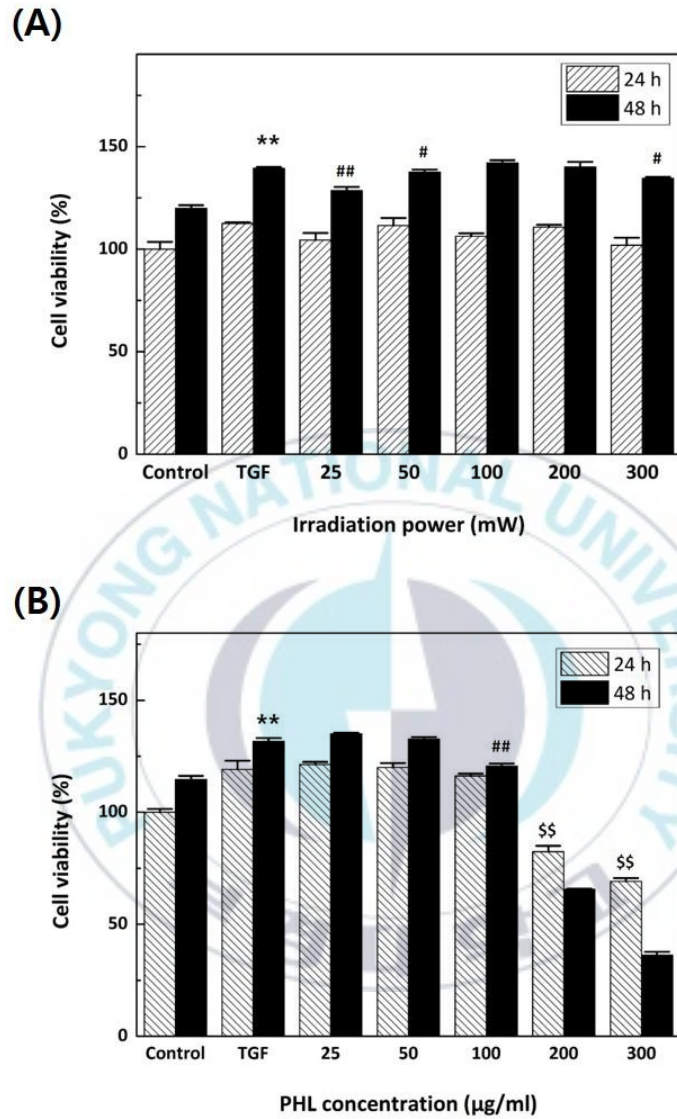


Figure 4. Cell viability of (A) low level laser therapy (635nm for 30 seconds) at various power levels and (B) phloroglucinol at various concentrations. (N= 6; \*\*P < 0.005 vs. control; \$\$P < 0.005 vs. TGF in 24 hours; #P < 0.05; and ##P < 0.005 vs. TGF in 48 hours).

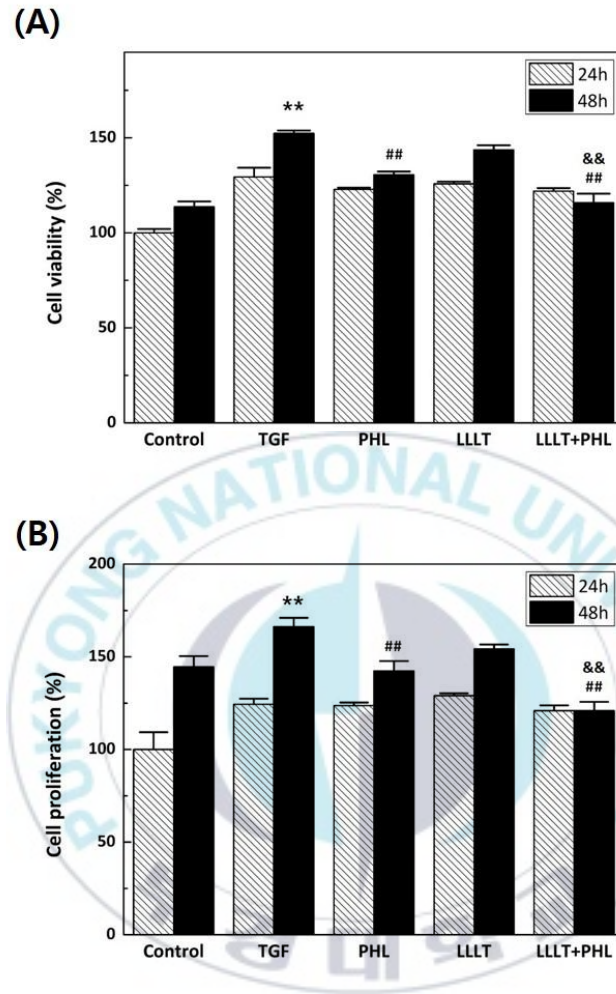


Figure 5. Effects of phloroglucinol assisted low level laser therapy (LLLT) on NIH/3T3 fibroblasts viability. (A) Cell viability and (B) proliferation was evaluated after 24 and 48 hours incubation. (N= 5; \*\*P < 0.005 vs. control; ##P < 0.005 vs. TGF; &&P < 0.005 vs. PHL).

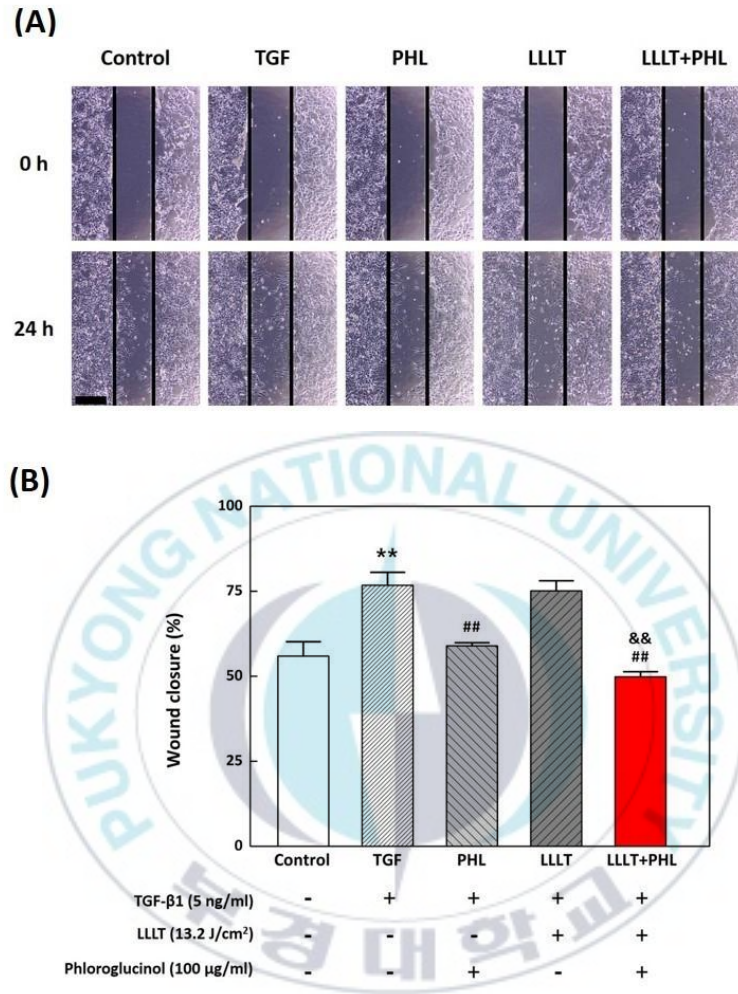


Figure 6. (A) Microscopic images captured at 0 and 24 hours after cell wounding and (B) wound closure rate measured by using wound closure (%) = Migration cell surface area/total surface area 100% (N= 3; \*\*P < 0.005 vs. control; ##P < 0.005 vs. TGF; &&P < 0.005 vs. PHL).

### 2.3.4. Gene expression of fibrotic markers

The expression levels of fibrotic markers, such as  $\alpha$ -SMA and type 1 collagen, were evaluated by immunofluorescence to confirm the differentiation of fibroblast cells. As shown by confocal imaging (Figure 7A),  $\alpha$ -SMA (green) and type 1 collagen (cyan) were considerably present in TGF groups compared to the control. However, the expression levels were significantly reduced in LLLT+PHL groups. Quantitative analysis showed greater than three times the expression of  $\alpha$ -SMA (Figure 7B) in TGF compared to the control. The expression level decreased in the PHL group ( $40.2 \pm 5.5$  %) and LLLT group ( $24.3 \pm 5.4$  %) compared to TGF. Type 1 collagen (Figure 7C) also increased more than four times in TGF compared to the control and decreased in the PHL group ( $39.1 \pm 3.8$  %) and LLLT group ( $22.9 \pm 5.2$  %). The LLLT+PHL groups were significantly reduced to  $67.5 \pm 3.1$  % in  $\alpha$ -SMA and  $57.1 \pm 0.6$  % in type 1 collagen compared to the TGF group. PHL-assisted LLLT minimized the over-expression of  $\alpha$ -SMA and type 1 collagen induced by TGF. To prove the modulating effect of protein expressions, western blot analysis was conducted. As shown in Figure 8A, although  $\alpha$ -SMA did not change significantly in 24 h, the  $\alpha$ -SMA levels increased in the TGF group (178 %) compared to the control in 48 h. Otherwise, the  $\alpha$ -SMA levels for the PHL (134 %), LLLT (135 %), and LLLT+PHL (91 %) groups were significantly decreased. The expression of TGF- $\beta$  (Figure 8B) increased in the TGF group (164 %) and decreased in the PHL (92.5 %), LLLT (101 %) and LLLT+PHL groups (73.5 %). The expression levels of type 1 collagen (Figure 8C) also increased in the TGF group (126 %) and decreased in the PHL (82.5 %), LLLT (105 %), LLLT+PHL groups

(39.5 %). To support these data, pro-collagen 1 was evaluated with an ELISA kit assay at 72 h (Figure 9). A standard ( $R^2 = 0.997$ ) and samples were measured twice. Pro collagen 1 increased in the TGF group (1083.9 pg/ml) compared to the control (554.8 pg/ml). However, the pro collagen 1 level was significantly reduced in the LLLT+PHL group (275.2 pg/ml) and decreased in the PHL (430.7 pg/ml) and LLLT groups (717.7 pg/ml). According to the results, PHL-assisted LLLT was the most effective in minimizing over-expression of fibrotic markers.



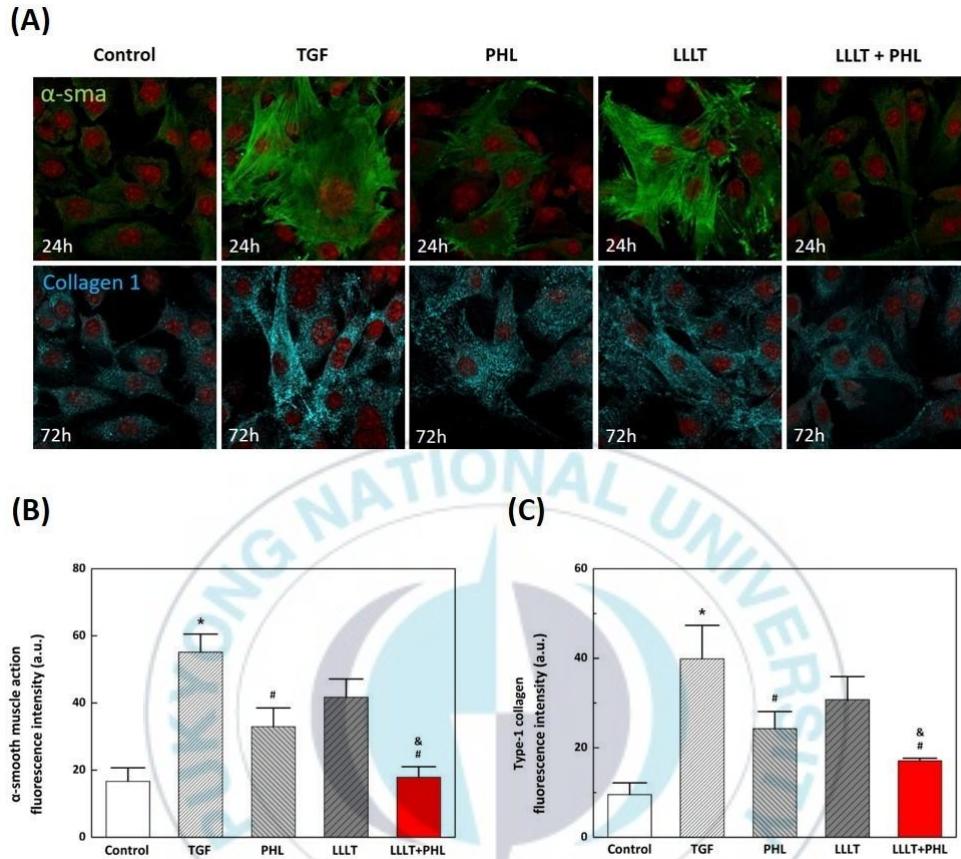


Figure 7. Effects of phloroglucinol assisted low level laser therapy (LLLT) on transition. (A) Fluorescence images of  $\alpha$  smooth muscle actin ( $\alpha$  SMA) (green at 24 hours) or type 1 collagen (blue at 72 hours). (B) The fluorescence intensity was analyzed by using fluorescence signals.

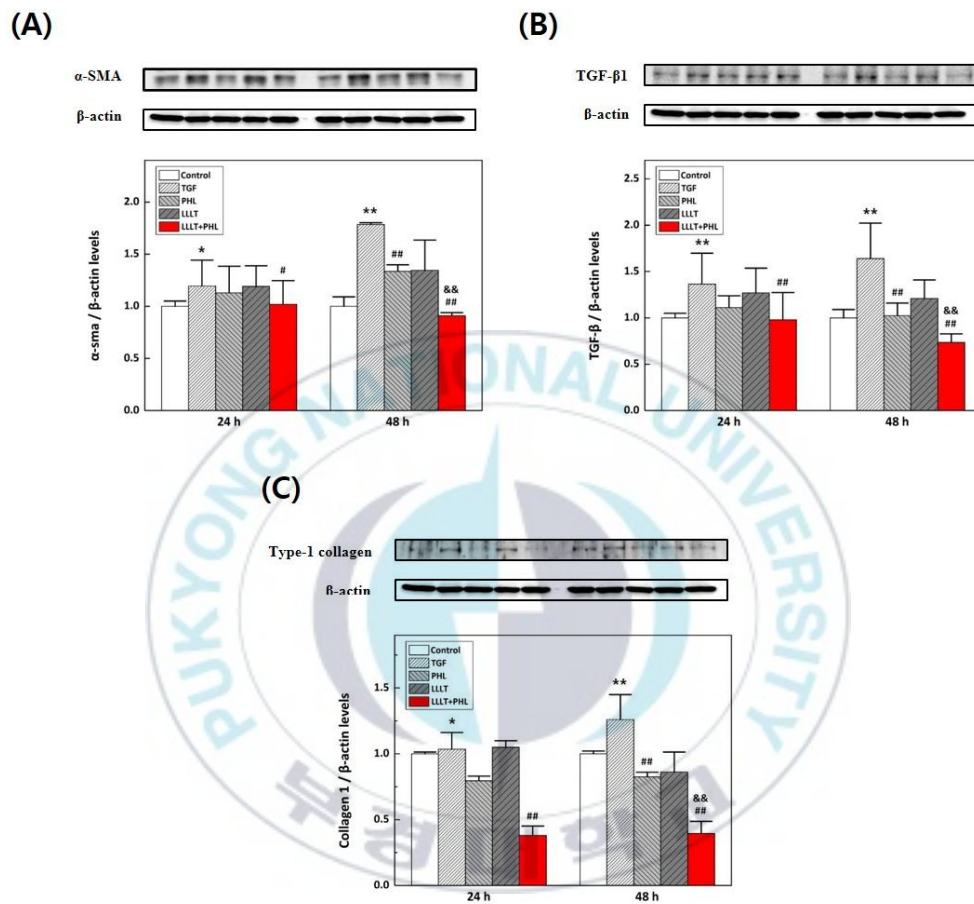


Figure 8. Effects of phloroglucinol assisted low level laser therapy (LLLT) on expressions of (A)  $\alpha$  smooth muscle actin ( $\alpha$  SMA), (B) transforming growth factor (TGF)  $\beta$ 1, and (C) type 1 collagen. (N= 5).

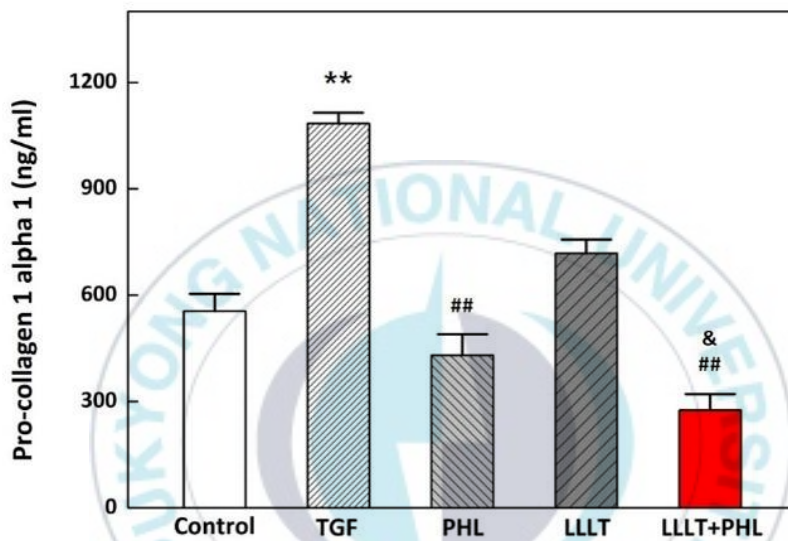


Figure 9. The expressions of pro collagen 1 alpha 1 and the major component of type 1 collagen were measured by using optical density (OD) values from the standard curve (N= 3; \*\*P < 0.005 vs. control; ##P < 0.005 vs. TGF; &P < 0.05 vs. PHL).

### **3. Effects of combined treatment of LLLT and phloroglucinol in a burn scar animal model**

#### **3.1. Purpose**

In worldwide, skin fibrosis is called scarring, and annually more than 100 million people suffer from the skin fibrosis [23, 24]. In previous in vitro study, we demonstrated the modulating effect of phloroglucinol-assisted LLLT on fibrotic condition. Based on the previous results, we investigated the feasible therapeutic effects of combined treatment in a burn scar animal model. It was hypothesized that LLLT with phloroglucinol could modulate the expression of fibrotic factors and eventually minimize scar tissue. The current study measured the wound size after combined treatment for comparing the wound healing effect. To identify the degree of the enhanced treatment, histological analysis was used to assess the skin thickness and collagen formation for re-epithelialization of scar tissue after treatment.

## 3.2. Materials and methods

### 3.2.1. Fabrication of burn scar animal model

The current study used a total of 20 male Sprague Dawley rats (age = 6 weeks, weight = 200 ~ 250 g, and five animals per group). Before the experiments, all the rats were anesthetized by applying intraperitoneal injection with zoletil and rompun in a 3:1 mixture solution (i.e., 0.4 cc per rat). Then, the back of each mouse was shaved using an electrical shaver, and then waxing cream was used to remove its hair completely. The animal experiments were approved by Institutional Animal Care and Use Committee at Pukyong National University (Number 2016–2030). A 1470 nm laser (FC-W-1470, CNI Optoelectronics Tech. Co., China) was used to fabricate the initial circular wound on the skin. The spot size was 0.3 cm<sup>2</sup> with 0.6 mm beam diameter. According to our previous study, 5 W of laser light was irradiated for 30 s to generate thermal wounds without any carbonization and induce thermally-induced scars after four weeks. A 600- $\mu$ m multimode optical fiber was vertically positioned 25 mm above the irradiation position. The power density was 16.7 W/cm<sup>2</sup>. To evaluate physical variations in the wound size, the wounded areas of each group were captured every days and Image J (National Institute of Health, Bethesda, MD) was used to achieve the quantitative data from the acquired image.

### 3.2.2. Laser and material treatment

Combined treatment was applied three days after irradiation 1470 nm laser for burn scar model. LLLT was conducted by using a visible laser system (SD-635-HS-1W, CNI laser, China) with a 635 nm wavelength in continuous-wave mode. A frontal light distributor (Medlight, Switzerland) with a beam diameter of 16 mm was used to irradiate the incident light in a uniform distribution. Before testing, the laser power was measured using a power detector (PD-300-3W, Ophir, Jerusalem, Israel) and power meter (Nova II, Ophir, Jerusalem, Israel). The laser light was irradiated for 160 s, 100 mW (8 J/cm<sup>2</sup>). PHL (GPR grade, MB-P4706, MB Cell, Seoul, Korea) was dissolved in distilled water (1 mg/ml) and filtered twice by using a membrane filter. 100 µl of PHL stock solution was treated by applying intramuscular injection. All treatments were conducted one time during experiment. All the groups were observed for 21 days after treatment. Experimental group = PT : phloroglucinol only, LT : LLLT only, and PLT : combined treatment (Figure 10).

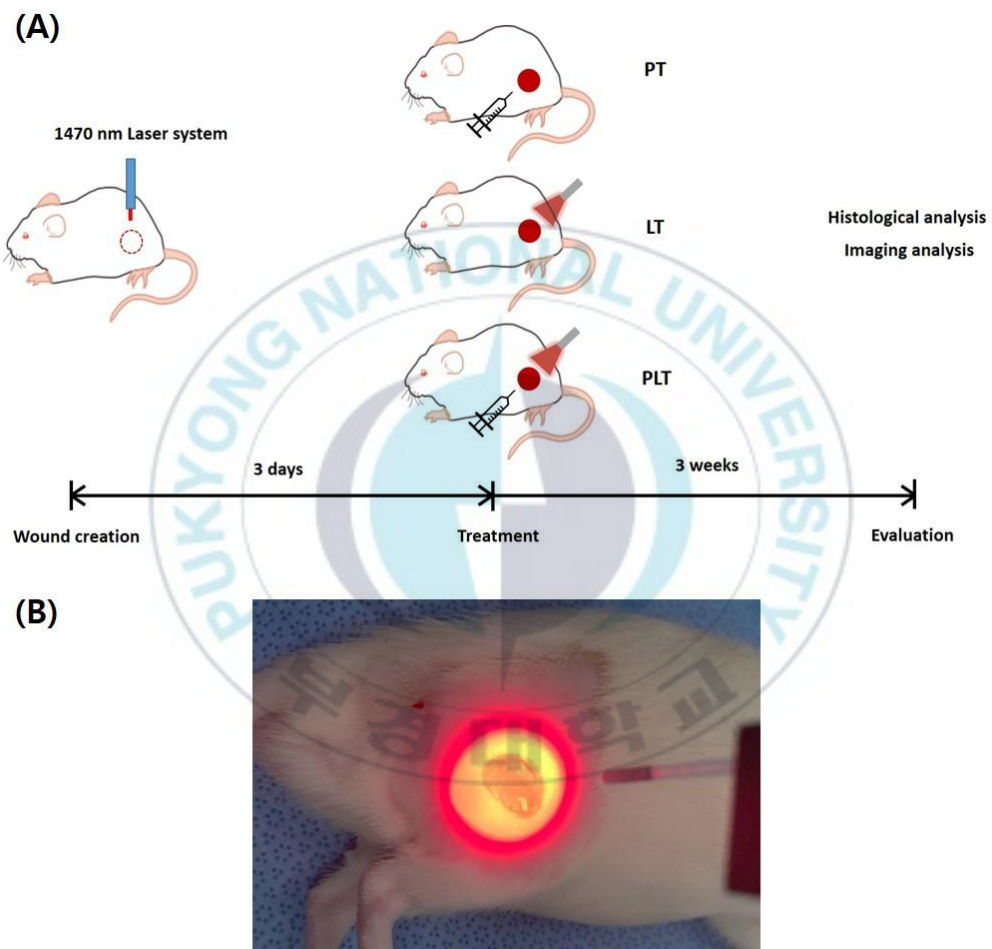


Figure 10. Experimental conditions and design for combined treatment in a burn scar animal model: PT (phloroglucinol), LT (LLLTT), and PLT (combined).

### **3.2.3. Histological analysis**

To evaluate histological changes, rats were euthanized on day 21 after treatment and scar tissues were harvested to observe histological variations. For fixation, the tissue sections were initially embedded in 10% formalin during 48 h. The paraffin blocks were made and sectioned by 6  $\mu\text{m}$  thickness to prepare histology slides. Hematoxylin eosin (H&E) staining were used to estimate the wound extent and wound healing progress. The collagen generation was also observed by Masson's trichrome (MT; American MasterTech, California, USA) staining. An optical microscope was utilized to observe the prepared slides and then, Image J was used to quantify the thickness of the physical injury and collagenous layers in a vertical direction along tissue depth.

### **3.2.4. Statistical analysis**

Statistical analysis was performed by using SPSS software 22 (SPSS Inc, Chicago, IL, USA), which calculated mean  $\pm$  standard deviation for at least three independent experiments. The Mann-Whitney U test was used for nonparametric statistical analysis, and significance was considered at  $p < 0.05$ .

### 3.3. Results

#### 3.3.1. Wound healing effect

To monitor progress of wound healing and scar formation, the wounded regions of all groups were captured at various time points (Figure 11). Overall, the wound size of all the groups decreased with the healing time, and the shape of wounds changed from circle to line after the complete healing (3 weeks). For quantitative analysis, wound area was measured by ImageJ (Figure 12). The initial wound size distribution were different for all the groups (Control =  $98.9 \pm 0.7$ , PT =  $96.2 \pm 1.1$ , LT =  $97.5 \pm 1.1$ , and PLT =  $97.8 \pm 0.7$ ). At day 3, the scab on the skin surface was removed, and all of wound size was slightly increased (Control =  $110.4 \pm 6.3$ , PT =  $109.7 \pm 3.4$ , LT =  $109.9 \pm 5.2$ , and PLT =  $113.1 \pm 1.0$ ). On week 1, PLT group ( $59.53 \pm 12.4$ ) was significantly decreased compared with the other groups. PT ( $79.1 \pm 14.6$ ) and LT ( $77.1 \pm 1.2$ ) were reduced more than control ( $84.6 \pm 6.3$ ). Two weeks later, the wound of PLT group ( $7.2 \pm 1.2$ ) was nearly closed. However, control ( $50.0 \pm 0.3$ ) was slightly reduced even similar as the PLT on week 1. PT and LT were decreased near  $22.2 \pm 1.2$  and  $17.6 \pm 5.6$ . Finally, all wounds were almost closed without significant difference after 3 weeks. (Control =  $1.9 \pm 0.1$ , PT =  $0.7 \pm 0.2$ , LT =  $0.7 \pm 0.1$ , and PLT =  $0.2 \pm 0.1$ )

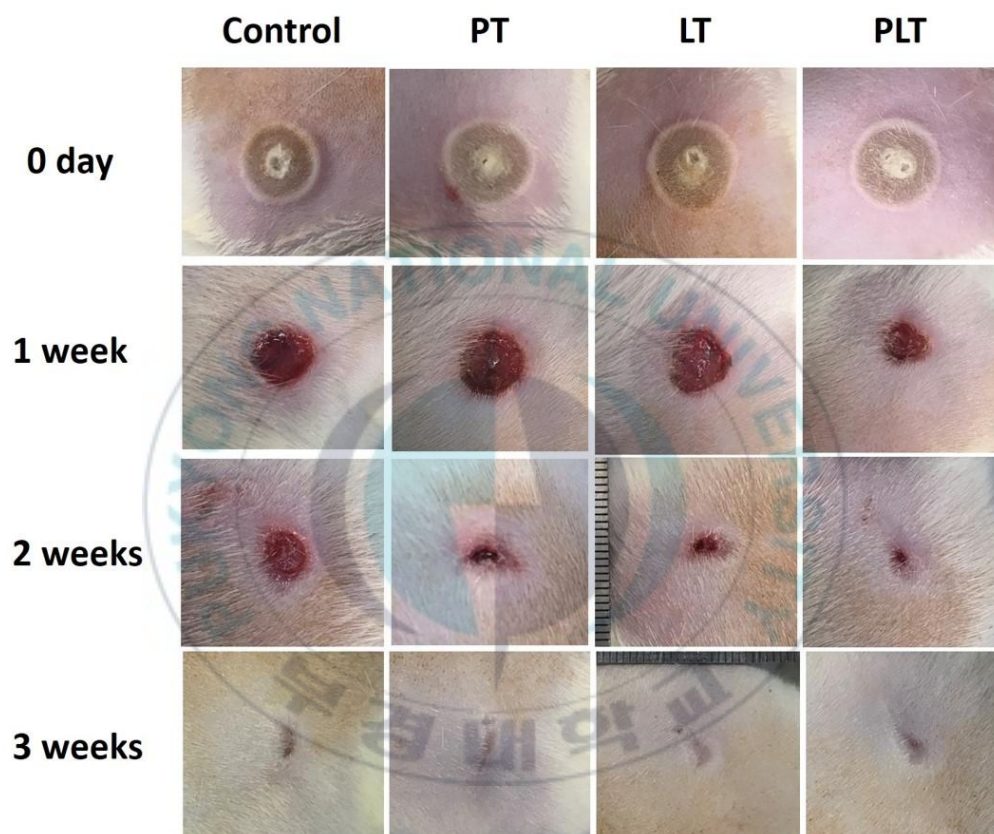


Figure 11. Top-view images of wound in burn scar animal model. Wound size was monitored and compared to evaluate wound healing effect of combined treatment.

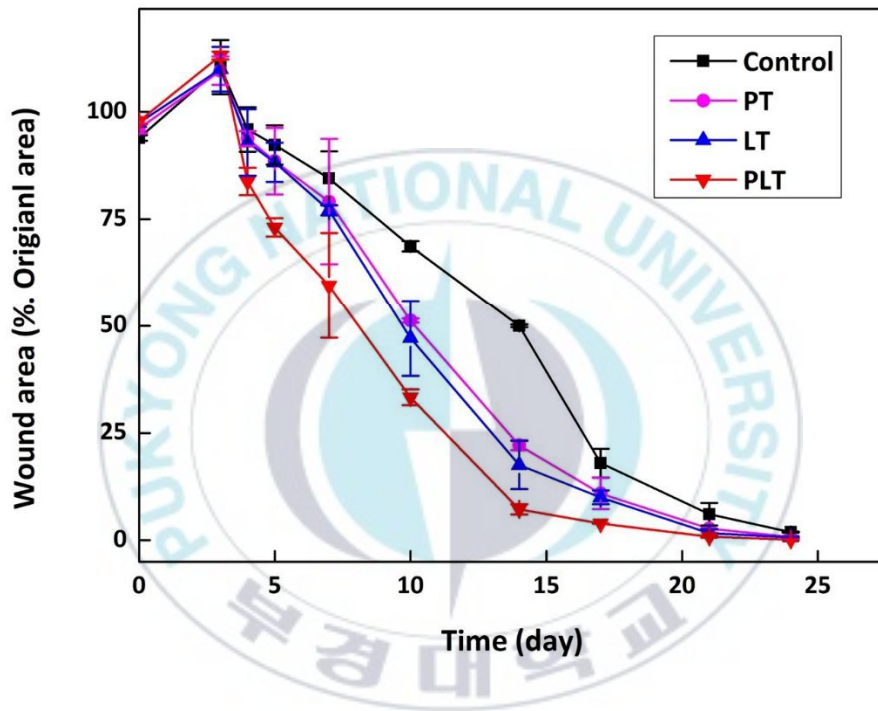


Figure 12. Comparison of wound size after combined treatment. (N=5 per group).

### 3.3.2. Comparison of skin thickness and collagen distribution

Figure 13 displays the histology images of normal tissue and the injured skin after 3 weeks. Normal skin shows loose collagen arrangement and rough layers of epidermis whereas all the groups resulted in high density of collagen that was horizontally oriented with the epidermal collagen fibers. Moreover, the epidermis from all the groups was smooth and thick due to scar formation. In particular, Control in Figure 13 induced thicker collagenous layers and higher collagen density, compared with the other groups. For quantitative evaluations of re-epithelialization, Figure 14 exhibits a comparison of the thickness of skin layers for the five groups. The epidermis was increased at PT ( $87.4 \pm 23.3$  mm) and LLLT ( $100.6 \pm 35.4$  mm) group compared to control. Otherwise, Control entailed almost twofold thicker epidermis ( $133.8 \pm 36.8$  mm) than PLT ( $68.9 \pm 23.3$  mm). The quantified thickness ratios confirmed that the remodeling of the epidermal layers was significantly uniform on PLT group. To evaluate the degree and distribution of collagen formation, Masson's trichrome was to stain the injured tissues for five groups (Figure 15). Collagen fibers (connective tissue) are represented as blue, nuclei as dark red/purple, and cytoplasm and muscle fibers as red/pink. Compared to normal skin, all groups on week 3 showed a larger collagen proportion, represented by dense blue layers below the epidermis. However, all treated groups showed minimal collagenous layer of epidermis and dermis compared with control group.

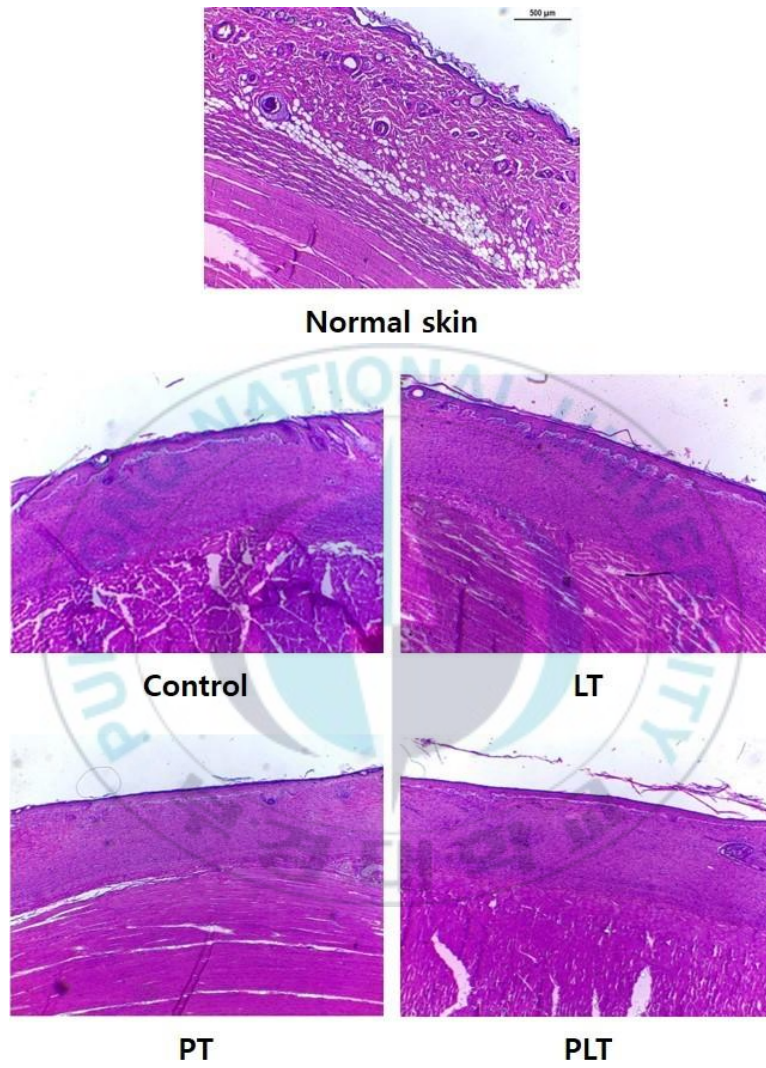


Figure 13. Hematoxylin and eosin staining of normal skin and treated tissues for histological features after 3 weeks.

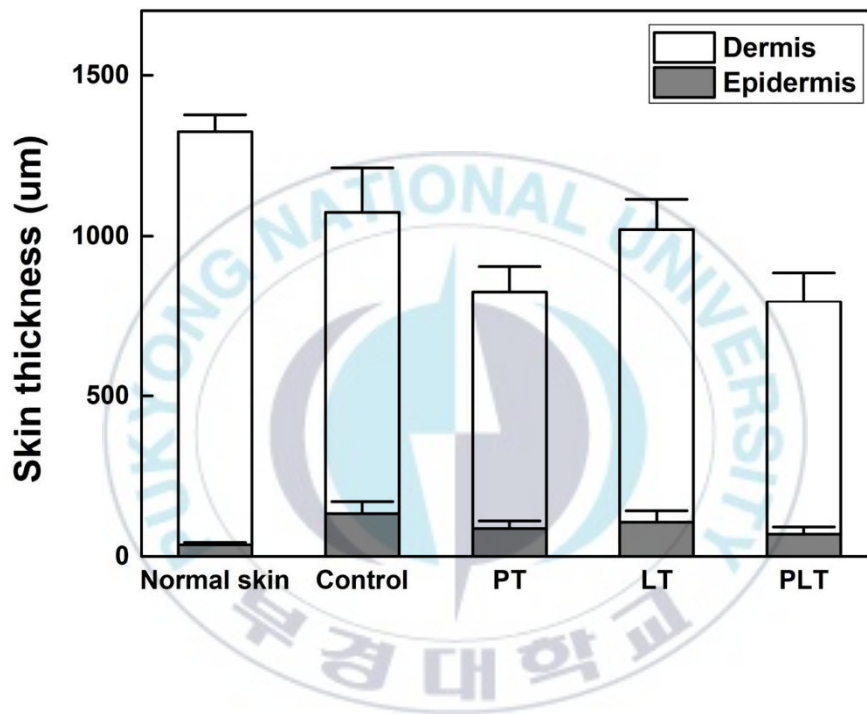


Figure 14. Quantitative analysis of skin layer thickness (dermis and epidermis) after 3 weeks.

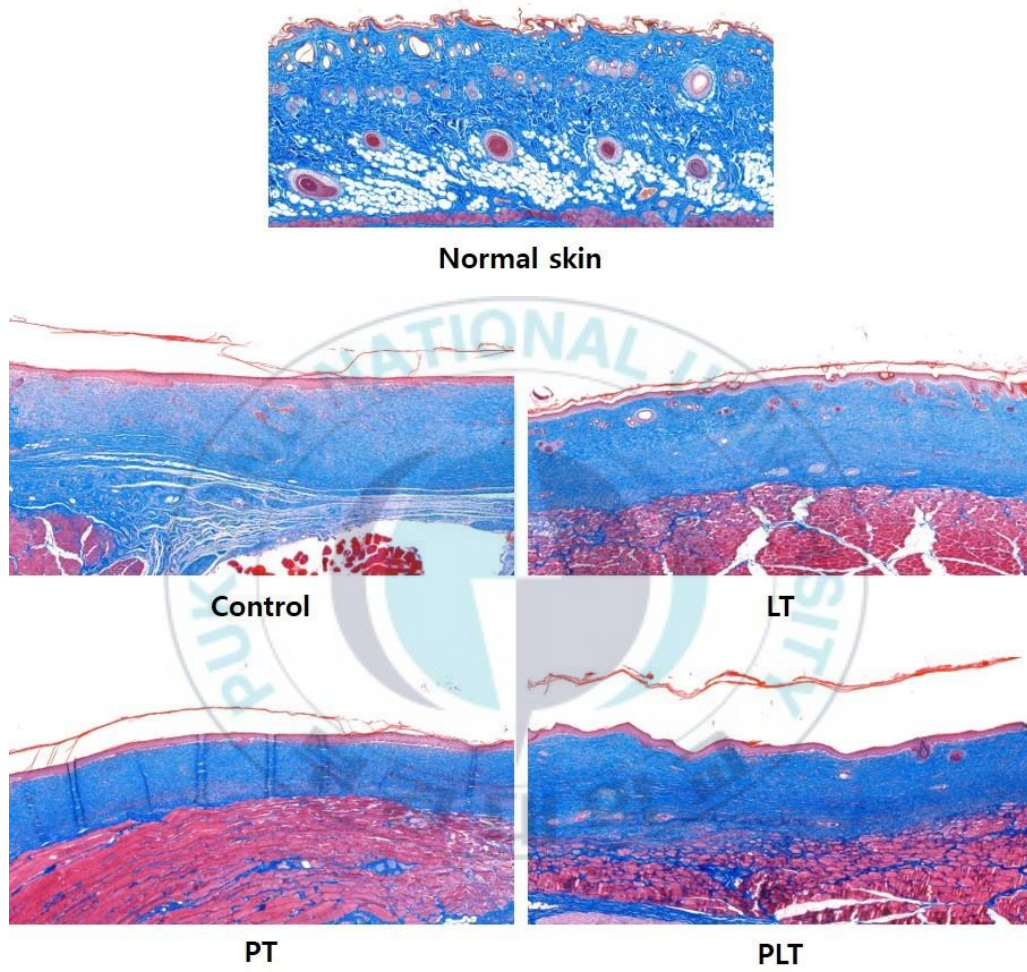


Figure 15. Masson's trichrome staining of normal skin and treated tissue for collagen formation after 3 weeks.

## 4. Discussion

Our research evaluated the inhibitory effects on fibrogenesis in vitro by applying PHL-assisted LLLT. MTT, BrdU and wound healing assays confirmed the modulating effects of proliferation and migration on MEF cells (Figures 4~6). In addition, PHL-assisted LLLT demonstrated additive modulation effects on fibrotic markers, such as  $\alpha$ -SMA, TGF- $\beta$ 1, and type 1 collagen according the results from immunofluorescence and western blots (Figures 7~9). Although, cell migration was delayed by combined treatment on MEF cells, wound healing speed was significantly promoted in in vitro (Figure 11~12). Moreover, the damaged tissue was remodeled with uniform epidermis layer similar to normal skin by combined treatment (Figure 13~15). Despite substantial research on scar management, the current fibrosis treatment is unable to effectively prevent progression and recurrence of the disease, and fibrosis treatment remains an unmet clinical need [1, 9, 25, 26]. Although several studies have shown enhanced effects on biological activity, research on inhibition effects is insufficient. The proposed combined therapy can be expected to have an advantage for inhibiting fibrosis and possibly preventing recurrence under long-term conditions compared with the current methods, such as bronchoscopic dilation and airway stenting, which provide short-term effects. Despite the inhibitory effects during wound healing and the initial fibrosis process, the proposed treatment should be further investigated with an advanced fibrotic state to show its therapeutic capability.

PHL, which is a water-soluble biocompatible marine material, could be easily applied to organs, such as the trachea, using a spray catheter in a solution state [27]. Previous studies demonstrated that PHL has anti-oxidant and anti-inflammatory effects [28]. PHL reduces the reactive oxygen species (ROS) and nitric oxide (NO) that regulate fibrotic markers, such as TGF- $\beta$  signaling [28-30]. One study also used phlorotannin (a complex polymer of PHL) to inhibit the MMP-2 and MMP-9 activities, which play important roles in the transition of fibroblasts to myofibroblasts [28]. Another study demonstrated that a natural antifibrotic compound called aspidin PB, a PHL derivative, can inhibit fibrogenesis by targeting TGF- $\beta$ 1 [31]. Aspidin PB effectively minimized type 1 collagen,  $\alpha$ -SMA, and TGF- $\beta$ 1 by blocking P13K/Akt signaling. Therefore, the marine material can be an effective pharmaceutical option for chemo-combined treatment of fibrosis.

LLLT may be a promising therapeutic method for various medical applications, such as a skin rejuvenation, muscle pain relief, and rhinitis treatment. In addition, LLLT is noninvasive and cost-effective like laser therapy using light-emitting diodes (LEDs). Previous studies demonstrated that irradiation of 635 nm light with a low intensity can modulate the transition of fibroblasts to myofibroblasts by reducing transient receptor potential canonical channel (TRPC) 1 and TGF- $\beta$ 1/Smad3 signaling [5, 9]. Another study indicated that LLLT at 808 nm can prevent fibrosis by decreasing the expression of TGF- $\beta$  and reducing collagen deposition [32]. Therefore, the combined therapy can

be easily and safely implemented by applying a biocompatible material and irradiating noninvasive LLLT to wound sites.

The current study showed additive effects of fibrosis inhibition by modulating TGF chemically and biologically to affect fibrotic factors. PHL chemically modulates the fibrosis process by binding to TGF receptors, which plays a key role in fibrogenesis. Otherwise, LLLT inhibited fibrosis through a biomodulation effect. A previous study reported that a combination of LLLT and Coenzyme Q10 accomplished additive enhancement of wound healing in diabetic rats, and the combined treatment accelerated both cell proliferation rates and hydroxyproline levels [33]. Another study also demonstrated an additive acceleration effect of full-thickness burn wound repair. The combination of 904 nm light and medicinal honey provided therapeutic efficacy by promoting proliferation and reducing inflammation in burn wound healing [34].

Although PHL was associated with additive modulation effect during LLLT, interactions of various marine materials with LLLT can lead to different responses in cells and tissues depending on the incident wavelength and fluence rate. In addition, several studies evaluated the reactions of natural and synthetic materials to laser irradiation. For example, photothermal therapy (PTT) and photodynamic therapy (PDT) uses thermal or chemical responses of the material to irradiation to promote treatment efficacy [35, 36]. Therefore, further investigations of various biocompatible materials with LLLT will be pursued to maximize biomodulation effects or to achieve more synergistic effects on the fibrosis process.

During the wound healing process, fibroblast transition induced by TGF and myofibroblast transition induced by TGF plays a key role in forming collagen and ECM. The current study aimed to modulate fibrotic factors as close to the normal healing process as possible with the combined therapy. It was confirmed that the individual treatments with PHL or LLLT may be effective in treating fibrosis by modulating TGF- $\beta$ , which leads to reduction of  $\alpha$ -SMA (a marker of myofibroblast) and collagen type 1 (a marker of ECM). The combined therapy advanced the TGF- $\beta$  modulating effects on fibrotic markers more effectively than individual treatments.

Although fibrotic markers showed additive treatment efficacy on fibroblasts, a limitation of the current study exists from the lack of identifying the cell signaling factors that underlie the therapeutic mechanism in the combined treatment. In this study, we used a black plate as background to minimize specular reflection. However, the heat effects of the LLLT from the photon-cell interaction was not verified. Although potential heat could be generated with  $\sim 100$  mW/cm<sup>2</sup>, the actual temperature change would be minimal. A recent study also reported that light-tissue interaction increased CCO, but hemodynamic and metabolic effects were not observed after pure thermal stimulation [37]. The future in vivo study will measure the real time temperature and metabolic responses to confirm any thermal effect. Although 635 nm might be quite effective for LLLT among various wavelengths (810, 850, 904, 980, and 1064 nm) due to its comparatively higher CCO absorbance in in vitro, high absorption of blood with wavelengths  $< 700$  nm would impede the efficacy of the 635 nm LLLT under in vivo

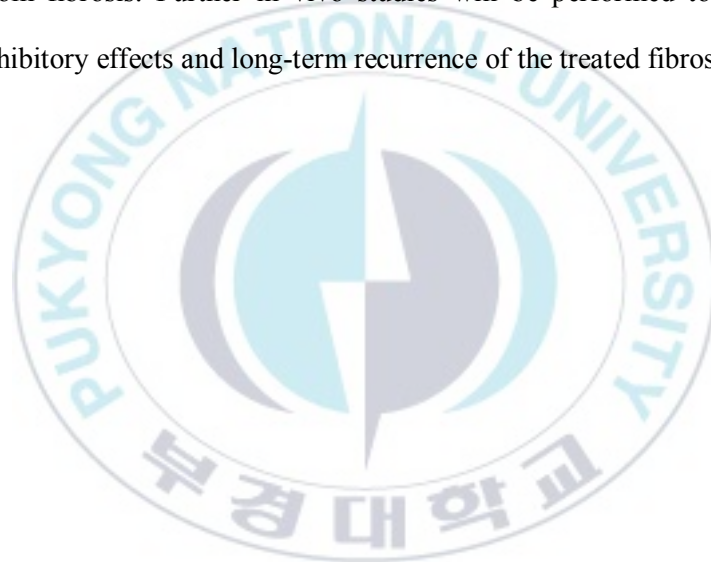
conditions. Thus, the further study still needs to evaluate various wavelengths to identify an appropriate wavelength for preclinical and clinical applications. In addition, the precise time of treatment is also need to compare for optimizing and enhancing the therapeutic effect. Another limitation is a decrease in the percentage of wound closure, as shown in Figure 6. Phloroglucinol-assisted LLLT showed a therapeutic effect on fibrotic problems, but it had a negative effect on cell migration that could affect wound healing. Therefore, the combined therapy should be developed to promote the wound healing while minimizing over-expression of fibrotic markers. Another limitation is that TGF- $\beta$  was used as a sole biological factor for the current evaluation. Other biological factors reacting with PHL and LLLT may lead to various responses, particularly in in vivo environments. To validate the safety and efficacy of the combined therapy for clinical translation, further in vivo testing is under way using animal models with skin scarring and trachea stenosis that were established in our previous studies [38-40]. The chronic response of tissue fibrosis after the combined treatment will be monitored to confirm the proposed therapeutic effect and to demonstrate the principal mechanism by immunohistochemistry and cell signaling analysis. In addition, for treatment of fibrosis in tubular tissue structures, such as the trachea and vocal cords, a spray catheter will be designed and developed to endoscopically deliver the PHL solution to the tissue lumen in in vivo test. A diffusing applicator will be used to irradiate tubular tissue with low-level light in a radial and uniform manner [41, 42]. Therapeutic doses for both PHL and LLLT will be quantified in terms of concentration

and fluence rate ( $J/cm^2$ ) to identify the optimal treatment conditions before in vivo testing.



## 5. Summary

In the present study, both in vitro and in vivo assessments were performed to investigate the antifibrotic effects of LLLT with phloroglucinol on murine embryonic fibroblast cells and rodent burn scar model. PHL-assisted LLLT could be an effective treatment to minimize the fibrotic problems by modulating TGF- $\beta$ 1. Moreover, the results of combined treatment has the potential to be an alternative treatment for patients suffering from fibrosis. Further in vivo studies will be performed to evaluate the proposed inhibitory effects and long-term recurrence of the treated fibrosis.



## 6. References

1. Wynn, T.A. and T.R. Ramalingam, *Mechanisms of fibrosis: therapeutic translation for fibrotic disease*. Nature medicine, 2012. **18**(7): p. 1028.
2. Lee, S.-Y., et al., *Successful treatment of tracheal stenosis with slide tracheoplasty after the failure of resection with end-to-end anastomosis*. Clinical and experimental otorhinolaryngology, 2009. **2**(4): p. 211.
3. Darby, I.A., et al., *Fibroblasts and myofibroblasts in wound healing*. Clinical, cosmetic and investigational dermatology, 2014. **7**: p. 301.
4. Bainbridge, P., *Wound healing and the role of fibroblasts*. Journal of wound care, 2013. **22**(8).
5. Mamalis, A., D. Siegel, and J. Jagdeo, *Visible red light emitting diode photobiomodulation for skin fibrosis: key molecular pathways*. Current dermatology reports, 2016. **5**(2): p. 121-128.
6. Chen, A.C., et al., *Low-level laser therapy activates NF- $\kappa$ B via generation of reactive oxygen species in mouse embryonic fibroblasts*. PloS one, 2011. **6**(7): p. e22453.
7. de Freitas, L.F. and M.R. Hamblin, *Proposed mechanisms of photobiomodulation or low-level light therapy*. IEEE Journal of selected topics in quantum electronics, 2016. **22**(3): p. 348-364.
8. Avci, P., et al. *Low-level laser (light) therapy (LLLT) in skin: stimulating, healing, restoring*. in *Seminars in cutaneous medicine and surgery*. 2013. NIH Public Access.
9. Sassoli, C., et al., *Low intensity 635 nm diode laser irradiation inhibits fibroblast–myofibroblast transition reducing TRPC1 channel expression/activity: New perspectives for tissue fibrosis treatment*. Lasers in surgery and medicine, 2016. **48**(3): p. 318-332.
10. Lev Tov, H., et al., *Inhibition of fibroblast proliferation in vitro using red light emitting diodes*. Dermatologic Surgery, 2013. **39**(8): p. 1167-1170.
11. Musumeci, A., et al., *Physical Therapy Modalities for Older Persons*, in *Rehabilitation Medicine for Elderly Patients*. 2018, Springer. p. 75-92.

12. Bensadoun, R.-j., *Photobiomodulation or low-level laser therapy in the management of cancer therapy-induced mucositis, dermatitis and lymphedema*. *Current Opinion in Oncology*, 2018. **30**(4): p. 226-232.
13. de Almeida, P., et al., *Red (660 nm) and infrared (830 nm) low-level laser therapy in skeletal muscle fatigue in humans: what is better?* *Lasers in medical science*, 2012. **27**(2): p. 453-458.
14. Wang, X., et al., *Interplay between up-regulation of cytochrome-c-oxidase and hemoglobin oxygenation induced by near-infrared laser*. *Scientific reports*, 2016. **6**: p. 30540.
15. Wang, X., et al., *Up-regulation of cerebral cytochrome-c-oxidase and hemodynamics by transcranial infrared laser stimulation: a broadband near-infrared spectroscopy study*. *Journal of Cerebral Blood Flow & Metabolism*, 2017. **37**(12): p. 3789-3802.
16. Hamblin, M.R. and T.N. Demidova. *Mechanisms of low level light therapy*. in *Mechanisms for low-light therapy*. 2006. International Society for Optics and Photonics.
17. Kim, M.-M. and S.-K. Kim, *Effect of phloroglucinol on oxidative stress and inflammation*. *Food and Chemical Toxicology*, 2010. **48**(10): p. 2925-2933.
18. Rauniyar, B.K., et al., *Anti-Stress Activity of Phloroglucinol: A Transient Metabolite of Some Plant Polyphenolics*. *Pharmacologia*, 2015. **6**(1): p. 21-30.
19. He, Y.-Q., et al., *Phloroglucinol protects the urinary bladder via inhibition of oxidative stress and inflammation in a rat model of cyclophosphamide-induced interstitial cystitis*. *Chinese medical journal*, 2015. **128**(7): p. 956.
20. Park, J., et al., *Effect of phlorotannins on myofibroblast differentiation and ECM protein expression in transforming growth factor  $\beta$ 1 induced nasal polyp derived fibroblasts*. *International journal of molecular medicine*, 2018. **42**(4): p. 2213-2220.
21. Treloar, K.K. and M.J. Simpson, *Sensitivity of edge detection methods for quantifying cell migration assays*. *PloS one*, 2013. **8**(6): p. e67389.
22. Puchkov, E.O., *Brownian motion of polyphosphate complexes in yeast vacuoles: characterization by fluorescence microscopy with image analysis*. *Yeast*, 2010. **27**(6): p. 309-315.

23. Bayat, A., D. McGrouther, and M. Ferguson, *Skin scarring*. Bmj, 2003. **326**(7380): p. 88-92.
24. Lim, A.F., et al., *The embrace device significantly decreases scarring following scar revision surgery in a randomized controlled trial*. Plastic and reconstructive surgery, 2014. **133**(2): p. 398.
25. Furuya, K., et al., *Pirfenidone for acute exacerbation of idiopathic pulmonary fibrosis: a retrospective study*. Respiratory medicine, 2017. **126**: p. 93-99.
26. Fiorucci, C., et al., *Su1053-Bar704, a Potent and Selective Fxr Agonist Protects Against Intestinal Fibrosis*. Gastroenterology, 2018. **154**(6): p. S-469.
27. Eom, J.S., et al., *Pleurodesis Using Mistletoe Extract Delivered via a Spray Catheter during Semirigid Pleuroscopy for Managing Symptomatic Malignant Pleural Effusion*. Respiration, 2018. **95**(3): p. 177-181.
28. Kim, M.-M., et al., *Phlorotannins in Ecklonia cava extract inhibit matrix metalloproteinase activity*. Life Sciences, 2006. **79**(15): p. 1436-1443.
29. Chang, M.-C., et al., *Antiplatelet effect of catechol is related to inhibition of cyclooxygenase, reactive oxygen species, ERK/p38 signaling and thromboxane A2 production*. PloS one, 2014. **9**(8): p. e104310.
30. So, M.J. and E.J. Cho, *Phloroglucinol attenuates free radical-induced oxidative stress*. Preventive nutrition and food science, 2014. **19**(3): p. 129.
31. Song, R., G. Li, and S. Li, *Aspidin PB, a novel natural anti-fibrotic compound, inhibited fibrogenesis in TGF- $\beta$ 1-stimulated keloid fibroblasts via PI-3K/Akt and Smad signaling pathways*. Chemico-biological interactions, 2015. **238**: p. 66-73.
32. Assis, L., et al., *Low-level laser therapy (808 nm) contributes to muscle regeneration and prevents fibrosis in rat tibialis anterior muscle after cryolesion*. Lasers in medical science, 2013. **28**(3): p. 947-955.
33. Mao, Z., et al., *Additive enhancement of wound healing in diabetic mice by low level light and topical CoQ10*. Scientific reports, 2016. **6**: p. 20084.
34. Yadav, A., et al., *Combination of medicinal honey and 904 nm superpulsed laser-mediated photobiomodulation promotes healing and impedes inflammation, pain in full-thickness burn*. Journal of Photochemistry and

- Photobiology B: Biology, 2018. **186**: p. 152-159.
35. Mou, J., et al., *Black titania-based theranostic nanoplatfom for single NIR laser induced dual-modal imaging-guided PTT/PDT*. Biomaterials, 2016. **84**: p. 13-24.
  36. Kim, H., et al., *Hypericin-assisted photodynamic therapy against anaplastic thyroid cancer*. Photodiagnosis and photodynamic therapy, 2018. **24**: p. 15-21.
  37. Wang, X., et al., *Impact of heat on metabolic and hemodynamic changes in transcranial infrared laser stimulation measured by broadband near-infrared spectroscopy*. Neurophotonics, 2017. **5**(1): p. 011004.
  38. Lee, H.S., et al., *Rabbit model of tracheal stenosis induced by prolonged endotracheal intubation using a segmented tube*. International journal of pediatric otorhinolaryngology, 2015. **79**(12): p. 2384-2388.
  39. Kim, M., H. Kim, and H.W. Kang, *Comparative evaluations of hypertrophic scar formation in in vivo models*. Lasers in surgery and medicine, 2018.
  40. Lee, H.S., et al., *Rabbit model of tracheal stenosis using cylindrical diffuser*. Lasers in surgery and medicine, 2017. **49**(4): p. 372-379.
  41. Pham, N.T., et al., *Real-time temperature monitoring with fiber Bragg grating sensor during diffuser-assisted laser-induced interstitial thermotherapy*. Journal of biomedical optics, 2017. **22**(4): p. 045008.
  42. Nguyen, T.H., et al., *Circumferential irradiation for interstitial coagulation of urethral stricture*. Optics express, 2015. **23**(16): p. 20829-20840.